Opt Quant Electron (2012) 44:355–372
DOI 10.1007/s11082-012-9544-5

Nonlinear optical absorption and optical rectification in near-surface double quantum wells: combined effects of electric, magnetic fields and hydrostatic pressure

S. Y. López · M. E. Mora-Ramos · C. A. Duque

Received: 4 October 2011 / Accepted: 5 January 2012 / Published online: 31 January 2012

Abstract The theoretical study of the combined effects of electric and magnetic fields and hydrostatic pressure on the nonlinear optical absorption and rectification is presented for electrons confined within an asymmetrical GaAs-$Ga_{1-x}Alx$ As double quantum well. The effective mass, parabolic band, and envelope function approaches are used as tools for the investigation. The electric field is taken to be oriented along the growth direction of the heterostructure and the magnetic field is applied parallel to the interfaces of the quantum wells. The pressure-induced mixing between the two lowest conduction bands is considered both in the low and high pressure regimes. According to the results obtained it can be concluded that the nonlinear optical absorption and rectification coefficients depend in a non-trivial way on some internal and external parameters such as the size of the quantum wells, the direction of applied electric field, the magnitude of hydrostatic pressure, the stoichiometry of the wells and barriers, and the intensity of the applied magnetic field.

Keywords Non-linear optical absorption · Non-linear optical rectification · GaAs-based near surface double quantum wells · Electric and magnetic fields · Hydrostatic pressure

1 Introduction

The optics of intersubband transitions in semiconducting heterostructures has become a subject of the utmost interest in the last three decades. Such transitions present some unique properties that have turned into the physical foundations of the design and fabrication of

S. Y. López · C. A. Duque
Instituto de Física, Universidad de Antioquia, 1226 Medellín, Colombia

M. E. Mora-Ramos (✉)
Facultad de Ciencias, Universidad Autónoma del Estado de Morelos, Ave. Universidad 1001, 62209 Cuernavaca, Morelos, Mexico
e-mail: memora@uaem.mx

novel optoelectronics devices. Numerous applied and basic research works on the matter can be found in the literature along these years.

Among the most attractive features of intersubband transitions one finds the large values of the oscillator strength and the small relaxation times (Baier et al. 1996). There are observations of rather high values of the oscillator strength in quantum wells (QW), which lead to large dipole moments of the associated optical transitions. Consequently, it is possible to predict the obtention of important nonlinear optical responses in semiconducting QW structures. We may refer to the observation of: second harmonic generation (Fejer et al. 1989), nonlinear optical absorption (NOA) and nonlinear optical rectification (NOR) (Rosencher et al. 1989), frequency down conversion (Sirtori et al. 1994), the dc Kerr effect (Sa'ar et al. 1992), and the third harmonic generation (Sirtori et al. 1992). These are all experimental reports, and they have motivated the realization of many theoretical studies regarding the optical nonlinearities in semiconductor heterostructures (Tsang et al. 1990; Rosencher and Bois 1991; Lien et al. 1994; Rosencher et al. 1996; Liu et al. 2000; Karabulut et al. 2007; Załużny 1993; Wei and Xie 2010; Karabulut et al. 2005; Baskoutas et al. 2007; Xie 2009; Duque et al. 2011a,b; Karabulut et al. 2011a; Karabulut and Duque 2011b; Kasapoglu et al. 2011). These studies show that the mentioned properties are—in QWs and quantum dots, for instance—closely related with asymmetries in the spatial dependencies of the energy states. Such asymmetries can be obtained via the application of electric fields, the variation of the stoichiometry of the well and barrier materials, the insertion of defects and some other mechanisms.

Finally, Eseanu (2011) and Niculescu and Eseanu (2011) have studied the exciton effects on the interband absorption spectra in differently shaped near-surface quantum wells with symmetrical/asymmetrical barriers under intense laser field taking into account the correct dressing effect for the confinement potential and electrostatic self-energy due to the repulsive interaction between carriers and their image charges. The infinite potential barriers have used to simulate the surface of the heterostructure, i.e., the GaAs-vacuum or $GaAl_{1-x}As_x$-vacuum interfaces.

The present article focuses on the study of the NOA and the NOR associated with an electron confined in a near-surface double asymmetrical QW (ADQW), under the combined effects of electric and magnetic fields together with the application of hydrostatic pressure. The calculations correspond to the so-called saturation limit, and the formalism includes the effective mass, parabolic bands, and envelope function approximations. The organization of the work is the following: Sect. 2 briefly presents the description of the theoretical model. In Sect. 3 one finds the corresponding results and discussion. Finally, Sect. 4 contains the main conclusions of the study.

2 Theoretical framework

Here we are considering the problem of an electron confined within a near-surface GaAs-$Ga_{1-x}Al_x$ As ADQW grown along the z-axis, under the simultaneous effects of electromagnetic fields (dc electric field oriented in the growth direction and homogeneous magnetic field applied perpendicularly to such orientation) as well as hydrostatic pressure. In the Landau gauge ($\mathbf{A}(\vec{r}) = -Bz\hat{y}$), the Hamiltonian operator for the electron in the heterostructure is given by the expression:

$$H = \frac{1}{2m_e^*(P)}\left(\vec{p} + \frac{e}{c}\mathbf{A}\right)^2 + V(z, P) - eFz, \tag{1}$$

where $\mathbf{A}$ is the vector potential associated to the magnetic field, $\vec{p}$ is the momentum operator, $\vec{r}$ is the vector position of the electron, and e is the absolute value of the electron charge. Additionally, the quantity $m_e^*(P)$ is the pressure-dependent effective mass of the electron, and $V(z, P)$ is the confining potential of the heterostructure which is also a function of the hydrostatic pressure.

The configuration of the near-surface ADQW considered is that of two quantum wells of widths L_{W1} and L_{W2} separated by a central potential barrier of width L_b. The origin of coordinates is taken at the middle point of the central barrier. The confining potential is infinite in the intervals $z < -L_{W1} - L_b/2$ and $z > L_{W2} + L_b/2$, it is $V(z, P) = V_0(P)$ within the interval $z < |L_b/2|$, and zero in the regions inside both wells. The near-surface effects have been considered via the vacuum-GaAs interface.

The hydrostatic pressure dependence of the potential energy is given by (Elabsy 1994):

$$V_0(P) = \begin{cases} \Gamma_b^{(P)} - \Gamma_w^{(P)}, & P \leq P_1 \\ X_b^{(P)} - \Gamma_w^{(P)}, & P > P_1, \end{cases} \tag{2}$$

where $\Gamma_w^{(P)}$, $\Gamma_b^{(P)}$, and $X_b^{(P)}$ are the minima of the conduction band at the points Γ and X of the Brillouin zone for the well (w) and barrier (b) material, respectively. These energies are measured with respect to the top of the valence band at the Γ point of the Brillouin zone, for the well material. The potential that confines the electrons in the conduction band of the system is taken as the 60% of the difference between the energy gaps of the barrier and well materials. In Eq. (2) P_1 (= 10 kbar when the Al molar fraction in the barrier material is $x = 0.3$) corresponds to the value of the hydrostatic pressure at which the intersection of the conduction $X_b^{(P)}$ and $\Gamma_b^{(P)}$ takes place. The electron effective mass is given by the expression (Raigoza et al. 2004):

$$\frac{m_e^*(P)}{m_0} = \left[1 + \frac{15020}{1519 + 10.7P} + \frac{7510}{1519 + 10.7P + 341}\right]^{-1}, \tag{3}$$

where m_0 is the free electron mass. The size of the heterostructure; that is, the widths of barriers and wells, can be obtained from the fractional change in the GaAs volume induced by the hydrostatic pressure (Raigoza et al. 2004).

Given the configuration of the heterostructure and the direction of the applied magnetic field, the component of the momentum operator in the QW plane is an exact integral of motion, with eigenvalue $\vec{T}_\perp$. Therefore, the eigenfunctions of the Hamiltonian in Eq. (1) can be written in the form

$$\Psi(\vec{r}) = \frac{1}{\sqrt{S}} \exp(i\, \vec{T}_\perp \cdot \vec{\rho})\, \phi(z). \tag{4}$$

In this expression S is the transversal area of the ADQW, $\vec{\rho}$ is the in-plane coordinate and $\phi(z)$ are the eigenfunctions of the confined electron motion with the Hamiltonian

$$H_c = -\frac{\hbar^2}{2\, m_e^*(P)} \frac{d^2}{dz^2} + V(z, P) + \frac{e^2\, B^2\, z^2}{2\, m_e^*(P)\, c^2} - e\, F\, z. \tag{5}$$

The way to calculating the eigenvectors—envelope functions—of H_c relies in a method developed by Xia and Fan (1989). The approach was later used in the calculation of optical absorption in superlattices under magnetic fields by de Dios Leyva and Galindo (1993). The scheme is based on the expansion of the electron states over a complete orthonormal basis of sine functions associated with a QW of infinite potential barriers.

Obtaining the energies and the corresponding envelope wave functions allows the calculation of the NOR and the NOA within the density matrix approach. The intensity-dependent NOA and NOR coefficients are given by (Lien et al. 1994; Rosencher and Bois 1991):

$$\alpha(\omega, I) = \alpha_{\max}\, G(\omega, I) \tag{6}$$

and

$$\chi(\omega, I) = \chi_{0,\max}\, G(\omega, I) \tag{7}$$

with

$$\alpha_{\max} = \alpha(\omega = \omega_{21}, I = 0) = \frac{e^2\, \gamma\, N_0\, \omega_{21}\, z_{21}^2\, T_2}{\hbar\, \varepsilon_0\, c\, n}\,, \tag{8}$$

$$\chi_{0,\max} = \chi_0(\omega = \omega_{21}, I = 0) = \frac{2\, e^3\, \gamma\, N_0\, z_{21}^2\, \Delta z_{21}\, T_1\, T_2}{\varepsilon_0\, \hbar^2}\,, \tag{9}$$

and

$$G(\omega, I) = \frac{\widetilde{\Gamma}_2^2}{(\delta^2 + \widetilde{\Gamma}_2^2)(1 + I/I_0)}\,, \tag{10}$$

where $z_{21} = \langle \phi_2 | z | \phi_1 \rangle$ and $\Delta z_{21} = |\, \langle \phi_2 | z | \phi_2 \rangle - \langle \phi_1 | z | \phi_1 \rangle\, |$. Also, ε_0 is the vacuum permittivity, n is the refractive index of the wells material, $\gamma\, N_0$ (with $0 < \gamma \leq 1$) is the tri-dimensional density of electrons in the heterostructure, $\Gamma_i = \hbar / T_i$ $(i = 1, 2)$, $\widetilde{\Gamma}_2^2 = \Gamma_2^2 (1 + I/I_0)$, $\delta = \hbar\omega - E_{21}$ (with $E_{21} = E_2 - E_1$, and $E_{21} = \hbar\, \omega_{21}$) is detuning, I is the intensity of the optical radiation, $I_0 = n \Gamma_1 \Gamma_2 / \left(2\, e^2\, z_{21}^2\, Z_0\right)$ is the optical saturation intensity, and Z_0 is the vacuum impedance (=120 $\pi\, \Omega$).

The quantity $\gamma\, N_0$, appearing in Eqs. (8) and (9), corresponds to the difference in the volume densities for the number of electrons of the ground (1) and first excited (2) states in the ADQW. We can evaluate it by means of the formula (Ahn and Chuang 1987)

$$\gamma\, N_0 = \frac{m_e^*\, k_B\, T}{\pi \hbar^2\, L} \ln \left\{ \frac{1 + \exp[(E_F - E_1)/k_B T]}{1 + \exp[(E_F - E_2)/k_B T]} \right\}, \tag{11}$$

which is a result of the summation over all values of the two-dimensional wavevector $\vec{k}_\perp = (k_x, k_y)$, with a parabolic dispersion relation. Here $L = L_{W1} + L_b + L_{W2}$ represents the total width of the ADQW heterostructure. The Fermi level E_F can be obtained—in the limit of near-zero temperature (T)—by means of the iterative procedure that solves the following equation:

$$E_F = \frac{1}{\eta} \left[\sum_{i=1}^{\eta} E_i + \frac{\pi \hbar^2 N_0\, L}{m_e^*} \right], \tag{12}$$

where η is the number of occupied levels within the ADQW.

3 Results and discussion

In this section we present the numerical results for the NOA and NOR in a GaAs-$Ga_{0.7}Al_{0.3}$As ADQW. The parameters used in our calculation are $T_1 = 1\,\text{ps}$, $T_2 = 0.2\,\text{ps}$, $N_0 = 8 \times 10^{24}\,\text{m}^{-3}$, and $n = 3.2$.

Before presenting the outcome of the calculation it is useful to perform an analysis of the changes in the energy states (Fig. 1) as well as in the tri-dimensional density of electrons

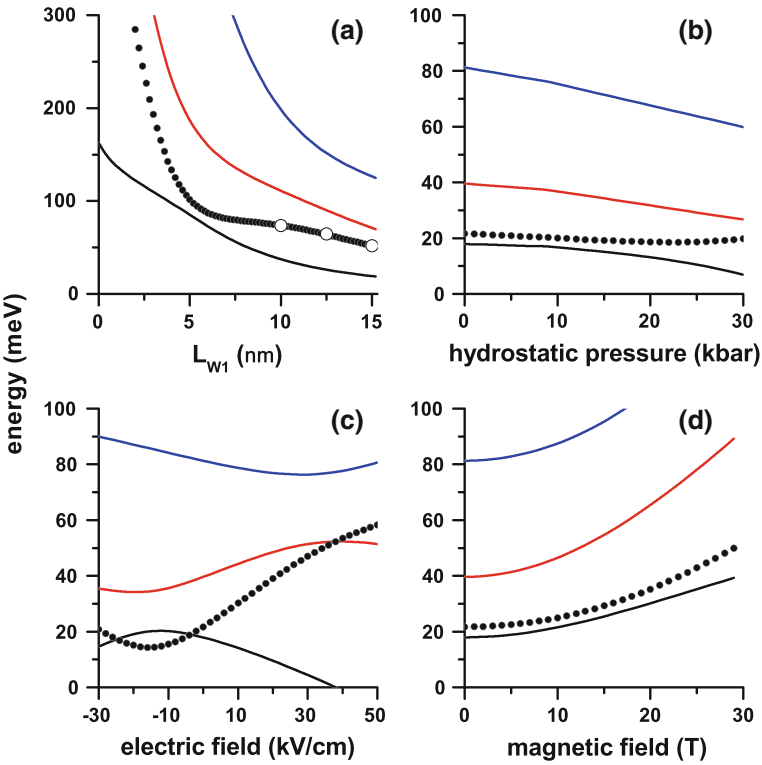

Fig. 1 Energy of the ground state and the two first excited states (*lines*) of a confined electron in an ADQW, with $L_b = 1$ nm. *Full dots* correspond to the energy difference between the ground state and the first excited state. For the parameters (L_{W1}, L_{W2}, P, F, B) the calculations are as follows: (variable, 5 nm, 0, 0, 0) **a**, (10 nm, 15 nm, variable, 0, 0) **b**, (10 nm, 15 nm, 0, variable, 0) **c**, (10 nm, 15 nm, 0, 0, variable) **d**. (Color figure online)

in the heterostructure (Figs. 2, 3) as a result of the variation of the main input parameters in the system. In Fig. 1 we show the behavior of the three lowest confined states in the ADQW as functions of the left hand side QW width, L_{W1}, (a); the hydrostatic pressure (b), the electric field (c), and the magnitude of the applied magnetic field (d). In all figures, the full dots represent the energy difference $E_2 - E_1$. Open symbols in Fig. 1a correspond to particular values of L_{W1} which will be the subject of detailed discussion below. As can be expected, the energies of the QW levels are decreasing functions of the total width of the system. Also, the variation of the E_i with respect to the hydrostatic pressure is a decreasing one, and this is mainly a consequence of the augment of the electron effective mass with P. On the contrary, the growth of the magnetic field intensity, B, leads to the increase of level energies. The reason for this effect lies in the strengthening of the confinement associated with the parabolic term in Eq. (5), thus pushing up the energy position of the levels. We observe a distinct situation in the monotonicity of E_i when these energies are evaluated as functions of the electric field. The difference in the behaviors of the first two QW states can be explained by analyzing the localization of the corresponding wave functions. For negative F (field oriented along the positive z direction), the probability density of the ground state confines mostly within the L_{W1} QW, and that of the first excited state largely locates within

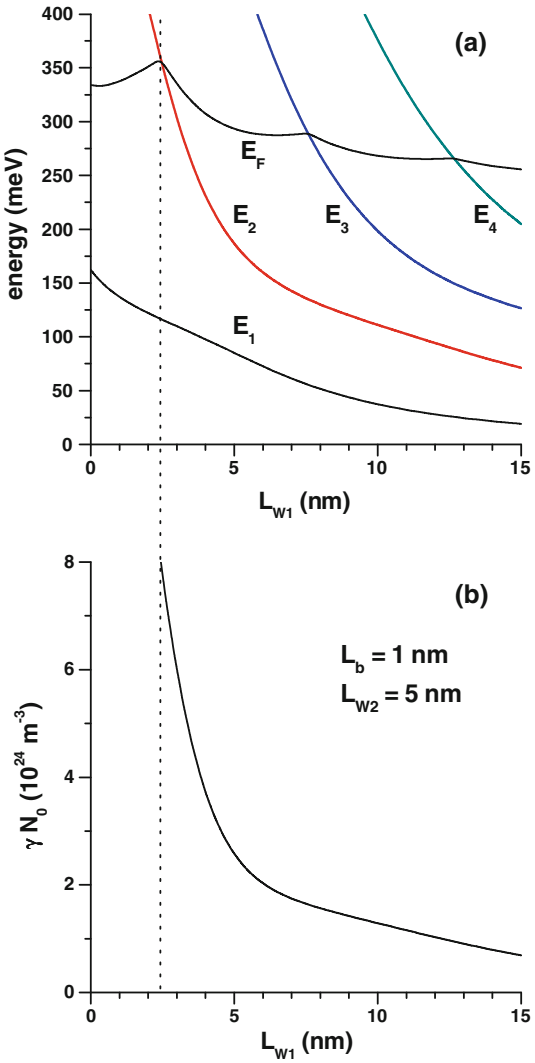

Fig. 2 The energies of the first four confined states as well as the calculated Fermi level position **a**; and the tri-dimensional density of electrons in the heterostructure **b**, as functions of the left hand side QW width in a GaAs-$Ga_{0.7}Al_{0.3}$ As ADQW. In both figures, the remaining parameters have the following fixed values: $L_b = 1$ nm, $L_{W2} = 5$ nm, $P = 0$, $F = 0$, $B = 0$, and $T = 4$ K. The *vertical dotted line* is just a guide to the eyes. (Color figure online)

the L_{W2} QW. The opposite happens when $F > 0$ [field oriented along $z < 0$, see Fig. 4c, d, e below for illustration]. If the electric field augments its magnitude in the negative sense [F approximately between 0 and -10 kV/cm], it starts an increase of the ground level due to the raising of the well bottom energy. But for larger negative F, the value of this energy begins to reduce due to the growth in the probability of tunneling of the electron towards de L_{W2} QW. Then, the effect of the infinite barrier at the left is less significant. This is also the reason for the variation of the first excited state, observed in the negative-F region of Fig. 1c. An analogous argument explains the variation of these energies in the positive-F region. For sufficiently large positive F (above 30 kV/cm) it is seen that there is again a change in the monotonicity of both levels. Once more, the reason for this result lies in the effect of the electric field upon the central barrier which enhances the probability of tunneling of the electron from one well to another.

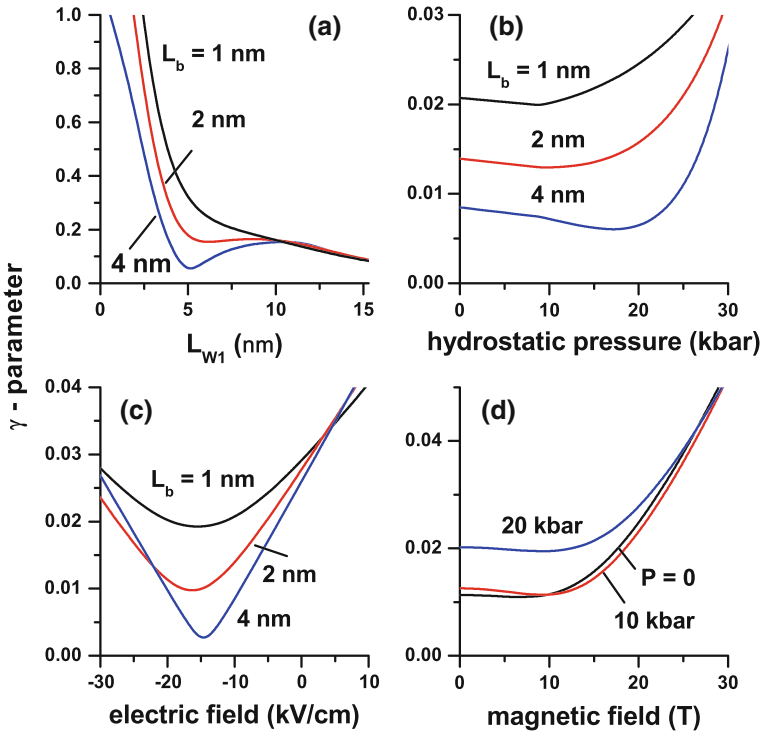

Fig. 3 The calculated γ-parameter in GaAs-$Ga_{0.7}Al_{0.3}$ As ADQW at $T = 4$ K. The results are distributed as follows: **a** the variation of γ as a function of L_{W1} for $L_{W2} = 5$ nm, $P = 0$, $F = 0$, and $B = 0$ including several different values of the central potential barrier width; **b** the evolution of the same parameter as a function of the hydrostatic pressure for $L_{W1} = 10$ nm, $L_{W2} = 15$ nm, $F = -10$ kV/cm, $B = 0$, and different values of the central barrier width; **c** γ as a function of the applied electric field for $L_{W1} = 10$ nm, $L_{W2} = 15$ nm, $P = 0$, $B = 0$, and the same set of values of the central barrier width; **d** the dependence of γ on the applied magnetic field with $L_{W1} = 10$ nm, $L_{W2} = 15$ nm, $L_b = 2$ nm, and $F = -20$ kV/cm, together with different values of the hydrostatic pressure. (Color figure online)

From the analysis of the Fig. 2 one notices that the volume electron density follows the same behavior of the energy difference $E_2 - E_1$, as a function of L_{W1}. This is in agreement with the limit $\gamma\, N_0 = \frac{m_e^*}{\pi\hbar^2 L}(E_2 - E_1)$, obtained from Eq. (11) at low temperatures.As long as the width of the first QW augments, the energy separation between the first two levels becomes smaller, and there will be a reduction in $\gamma\, N_0$. The peaks observed in the curve corresponding to the Fermi level position are related with the values of L_{W1} at which each of the upper electronic subbands in the system has filled with electrons. The reader may readily notice that precisely at the point in which the first excited subband becomes populated, the parameter γ is identically unity and the 3D electron density associated with the intersubband transition is exactly equals to N_0 (see the dotted vertical line in the figure as a guide to the eyes).

On the other hand, the Fig. 3 is drawn in order to help the understanding of the results contained in the subsequent graphics (Figs. 4, 5, 6, 7). Among other things, it includes the four sets of—varying and fixed—parameters used in the obtention of each of those figures. It is worth noticing that in the figures b–d, the results for γ are in the order of 0.01. This means that values of the electron density around 10^{22} m^{-3} are suitable for the study

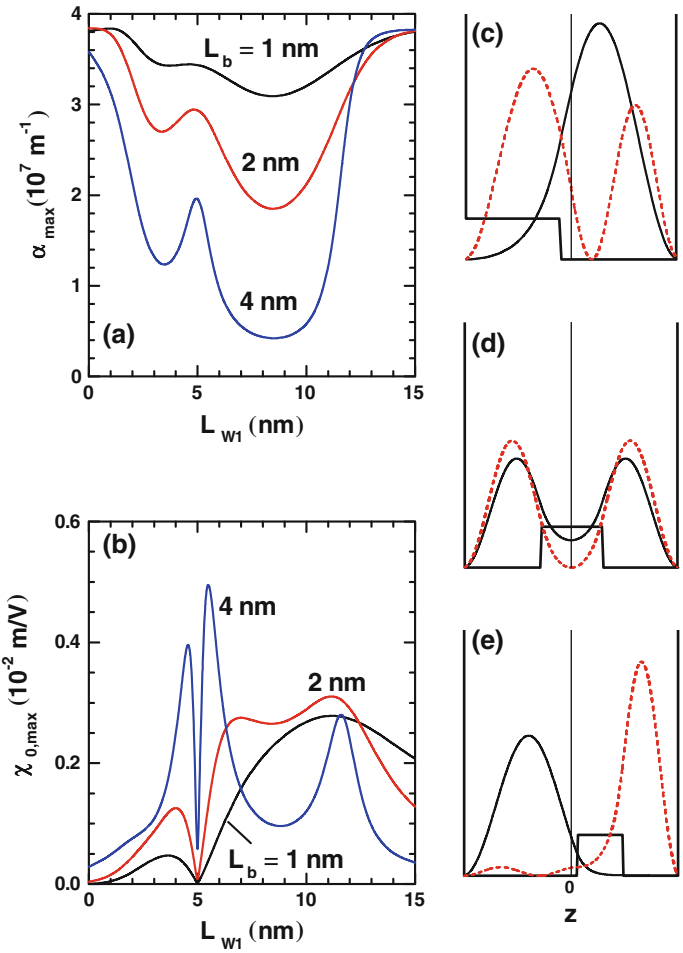

Fig. 4 Variation of the resonant peak values of the NOA (**a**) and the NOR (**b**) as a function of the width of the left hand side QW in a GaAs-$Ga_{0.7}Al_{0.3}$ As ADQW. In both figures, the fixed values of the parameters considered are $L_{W2} = 5$ nm, $P = 0, F = 0, B = 0$ together with several different values of the central potential barrier width. **c**, **d**, **e** show the z-direction densities of probability for the ground (*solid lines*) and first excited (*dashed lines*) states with $L_{W1} = 0$, $L_{W1} = 5$ nm, and $L_{W1} = 10$ nm respectively; considering $L_{W2} = 5$ nm and $L_b = 4$ nm. (Color figure online)

of the nonlinear optical properties in this kind of systems, as it has been already put forward in some of our previous works on the subject (Karabulut et al. 2011a). The behavior of the γ parameter is a suitable indicator of what is occurring with the energy separation between the first two confined levels as long as the external probes change their values. It is also interesting that, according to the Fig. 2a–d [except for $L_{W1} < 5$ nm in 2a], we will be able to calculate these optical properties in the whole range of sizes and external probe magnitudes without a restriction related with the amount of electrons per unit volume in the system, since in no case the value of γ reaches the unity.

We should also highlight that there is a detail in the calculation of the Fermi level position. We need to measure the energies entering the Eq. (12) with respect to the QW bottom. But in

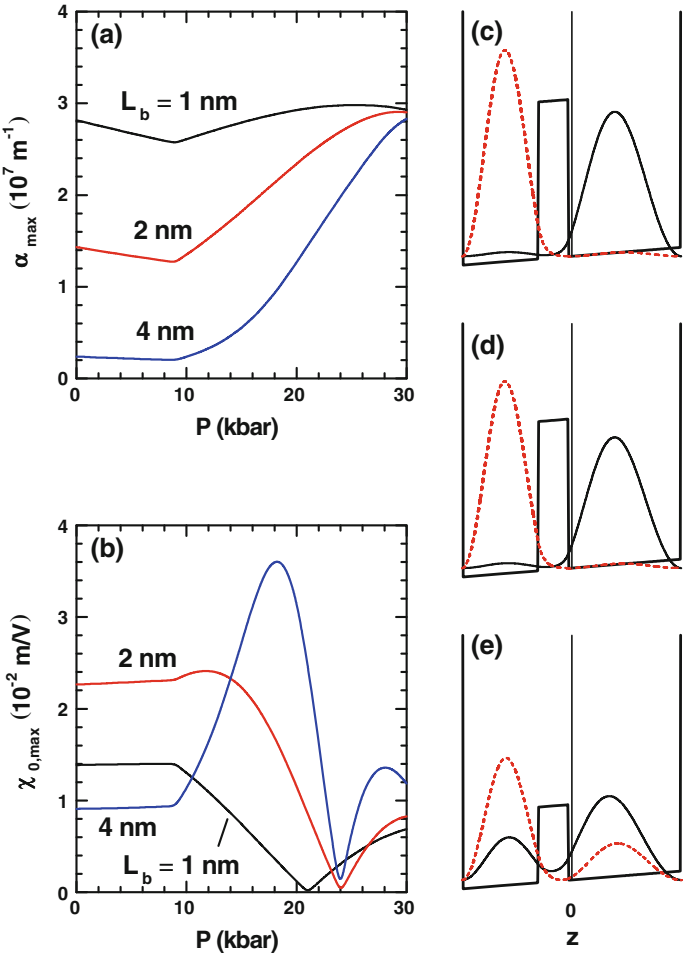

Fig. 5 The variation of the NOA (**a**) and NOR (**b**) resonant peaks as functions of the hydrostatic pressure in a GaAs-$Ga_{0.7}Al_{0.3}$ As ADQW. In both figures, the set of parameters considered are: $L_{W1} = 10$ nm, $L_{W2} = 15$ nm, $F = -10$ kV/cm, and $B = 0$. Different values of the central barrier width are included. **c**, **d**, **e** present the probability densities along the z-direction for the ground (*solid lines*) and first excited (*dashed lines*) states with $P = 0$, $P = 10$ kbar, and $P = 20$ kbar, respectively, considering $L_b = 4$ nm. (Color figure online)

the case that there exists an electric field we should locate the bottom of the well according to its field-induced displacement. This is done with the aim of avoiding the inclusion of negative values of the energy [see, for instance, the evolution of the lowest curve in Fig. 1c] in that equation.

The Fig. 4 contains the results of the variation of the height of the resonant peaks of the NOA (a) and NOR (b) coefficients in a GaAs-$Ga_{0.7}Al_{0.3}$ As ADQW depending on the width of the left QW [the configuration depicted in figures c–e]. For $L_{W1} = 0$ the resonant peak of the NOA, $\alpha_{\max}$, and the resonant peak of the NOR, $\chi_{0,\max}$, take different values for the three distinct central barrier widths considered. As long as L_b augments one can see that, with $L_{W1} = 0$, the system tends to behave as a single QW whose effective width grows as a function of L_b in the form $L_{W2} + L_b$. This is analogous to the inclusion of a kind of

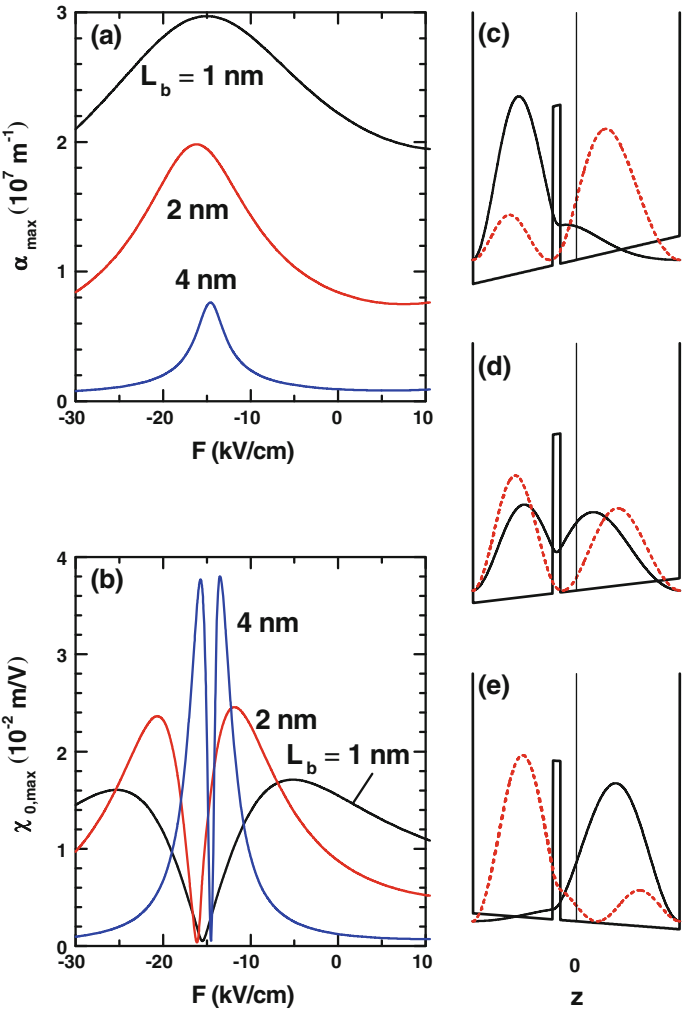

Fig. 6 Variation of the NOA (**a**) and NOR (**b**) resonant peak values as functions of the applied electric field, F, in a GaAs-$Ga_{0.7}Al_{0.3}$ As ADQW. In both figures the parameters considered are: $L_{W1} = 10$ nm, $L_{W2} = 15$ nm, $P = 0$, and $B = 0$. Several values of the width of the central potential barrier has been also included. **c**, **d**, **e** present the densities of probability along the z direction for the ground (*solid line*) and first excited (*dashed line*) states; with $F = -30$ kV/cm, $F = -15.5$ kV/cm, and $F = 10$ kV/cm, respectively. The value of the width of the central barrier is taken to be $L_b = 1$ nm. (Color figure online)

defect of width L_{W2}. The result is a displacement of the confined states towards the lower energies. The presence of L_b —which provides a finite barrier at the left of the L_{W2} QW—, reflects through the lack of even and odd symmetry in the ground and first excited eigenstates, relative to the center of that well ([see Fig. 4c]). For that reason, $\chi_{0,\max}$ is also different from zero when $L_{W1} = 0$. When $L_{W1} = 5$ nm, the system corresponds exactly to a symmetric double QW. As a consequence, the wavefunctions of the ground and first excited states have well defined symmetry with respect to $z = 0$ [see Fig. 4d], leading to $z_{11} = z_{22} = 0$. Thus, $\chi_{0,\max}$ is null. It is worth noticing that, associated with this zero value of $\chi_{0,\max}$, the peak α_{max} has a maximum at the same value of L_{W1}. These two critical values in α_{max} and $\chi_{0,\max}$

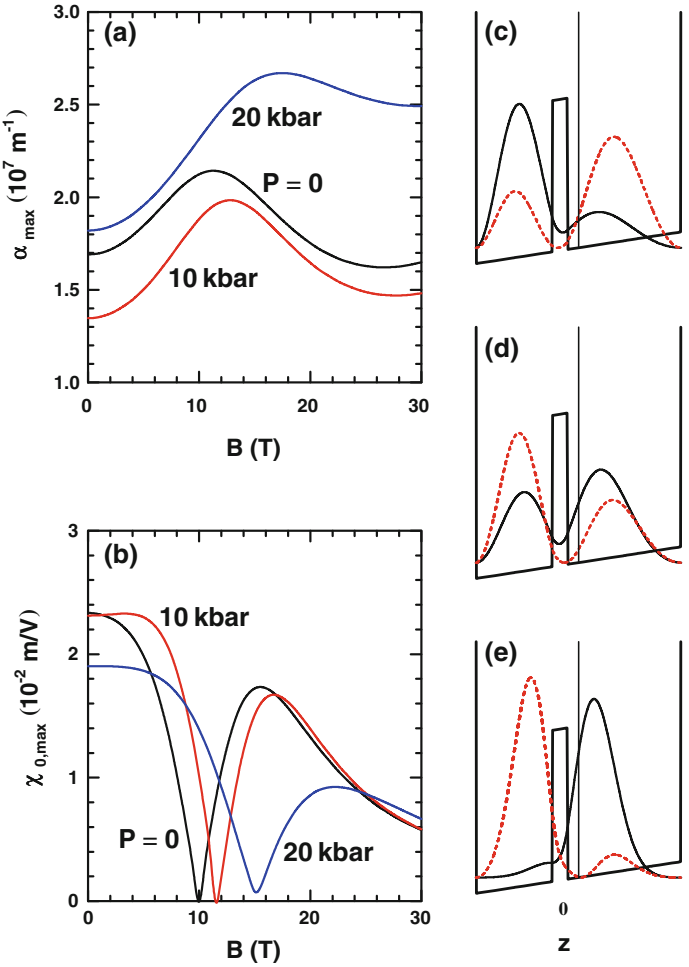

Fig. 7 Variations of the NOA (**a**) and the NOR (**b**) coefficients with the magnetic field strength, B, in a GaAs-$Ga_{0.7}Al_{0.3}$ As ADQW. For both figures we have $L_{W1} = 10$ nm, $L_{W2} = 15$ nm, $L_b = 2$ nm and $F = -20$ kV/cm, with different values of the hydrostatic pressure considered. The electronic densities of probability along the z-direction can be seen in **c**, **d** and **e** for the ground (*solid lines*) and first excited (*dashed lines*) states; with $B = 0$, $B = 12$ T, and $B = 30$ T, respectively. $P = 0$. (Color figure online)

(maximum and zero, respectively) can be observed for all the values of the central barrier width considered at exactly the same value of L_{W1} on the horizontal scale.

It must be noticed that the shape of the $\alpha_{\max}$ and $\chi_{0,\max}$ lines looks much alike for the different values of the barrier width. The shift of $\alpha_{\max}$ towards lower values as long as L_b increases is readily apparent and is due to the reduction in the value of ω_{21}. The increase of L_b causes the augment of the effective width of the double QW. As a result of this, it appears a decreasing of the electron confinement which makes the energy separation between the two involved states to be smaller. It is important to highlight that for small L_b the wavefunctions of the ground and first excited states [the ground state mostly localized within the wider well and the first excited state localized mostly within the narrower well —see Fig. 4e] are affected by the infinite barriers at both ends of the structure. On the other hand, when the value of L_b

becomes even larger the confinement over each one of the functions is associated with the effect of one infinite and one finite barriers. Clearly, if L_b tends to infinity we recover the case of two uncoupled asymmetric QW, causing the overlap between the first two states to become null. This would finally lead us to obtain the limit of $\alpha_{\max} = 0$.

The growing shape of $\alpha_{\max}$ in the region of values $L_{W1} > 10\,\text{nm}$ relates with the tendency of the system to behave as an isolated asymmetric QW of effective width equals to L_{W1} with infinite potential barrier at $z = -L_b/2 - L_{W1}$ and a finite potential barrier at $z = -L_b/2$. Such behavior as a single QW can be predicted by the simultaneous tendency of $\chi_{0,\max}$ towards zero, when $L_{W1} = 15\,\text{nm}$ in the curves with $L_b = 2\,\text{nm}$ and $L_b = 4\,\text{nm}$. As an important element of this discussion, we should mention that for $L_{W1} > 10\,\text{nm}$ the first two states of the double well system exhibit energies which are lower that the ground state of an isolated asymmetric QW of width $L_{W2} = 5\,\text{nm}$. For instance, in the particular case of $L_{W1} = 10\,\text{nm}$, $L_{W2} = 5\,\text{nm}$, and $L_b = 4\,\text{nm}$ the values of energies of the two lowest states in the system are 7.4 meV and 22.0 meV; whilst in the case with $L_{W1} = 0\,L_{W2} = 5\,\text{nm}$, and $L_b = 4\,\text{nm}$ those energies are 22.6 meV and 74.3 meV. This is related with the fact that the maxima of the probability densities of the ground and first excited states of the double well system mostly localize in the region of the L_{W1} well, when $L_{W1} > 10\,\text{nm}$. This causes an augment of the overlap between the wavefunctions and, therefore, to an increase in the value of the factor z_{21}^2.

Regarding the shape of the $\chi_{0,\max}$ line in the figure, it must be emphasized that it is basically associated to the factor Δz_{21}, which is slightly modulated by the term z_{21}^2. The three maxima in $\chi_{0,\max}$ are very well defined in the cases of $L_b = 2\,\text{nm}$ and $L_b = 4\,\text{nm}$. From left to right, the first and third peak maxima are due to maxima of the factor Δz_{21}. The second peak maximum is a consequence of a minimum in Δz_{21} which turns into a maximum due to the squaring.

In Fig. 5 the results for the variation of the NOA (a) and NOR (b) resonant peak values are shown as functions of the hydrostatic pressure in a GaAs-$Ga_{0.7}Al_{0.3}$ As ADQW.

In this particular case, the asymmetric configuration of the QW chosen implies that the negative electric field favors the recovery of the even and odd symmetries of the wavefunctions. For $P = 0, \alpha_{\max}$ diminishes with the augment of the central barrier width, just as in the case of $F = 0$ in Fig. 4. As we mentioned above, this is a consequence of the decrease of ω_{21} due to the loss of confinement for electrons. That is, the maximum of the density of probability moves away from the potential barrier located at $z = -L_{W1} - L_b/2$. The opposite situation happens to $\chi_{0,\max}$, at least in the situation in which $L_b \leq 2$ nm. This quantity increases with the barrier width.

For the ADQW configuration under the effect of a negative electric field and zero pressure, the growth of the barrier width produces a positive increase of z_{11} and a negative increase of z_{22}; which means that the absolute value of the difference $|\Delta z_{21}|$ increases as a result of the widening of the separating barrier. When $P = 0$, this feature results in the augment of $\chi_{0,\max}$ as a function of L_b. It is possible to observe the same behavior in z_{11} and z_{22} for $L_b > 2$ nm, but the sharp drop in $\chi_{0,\max}$ obeys the significant fall in the value of z_{21} which comes from the strong uncoupling of both QW for larger L_b.

When the pressure is augmented from 0 to 10 kbar the height of the central barrier remains constant and the effective mass is an increasing function of P. Since there are not variations in the degree of confinement and in the geometry of the heterostructure, there will not be any changes induced on the wavefunctions of the ground and first excited state [compare the densities of probability in the Fig. 5c, d]. Therefore, within this range of pressures the values of $|z_{21}|$ and z_{21}, and consequently that of $\chi_{0,\max}$ are merely constants as can be seen from

Fig. 5b. The augment of the effective mass makes the factor ω_{21} to become a decreasing function of P. Hence, as it is shown in Fig. 5a, $\alpha_{\max}$ linearly diminishes.

Because of the asymmetric character of the heterostructure, the value of $\chi_{0,\max}$ is different from zero for $P = 0$. However, the effect of the pressure-induced reduction of the barrier height [compare the potential barriers of Fig. 5d, e], the application of a constant electric field may be enough to force the fulfillment of the condition $z_{11} = z_{22}$; with which $|\Delta z_{21}| = 0$. This can be observed from the fact that $\chi_{0,\max}$ becomes null at $P = 21$ kbar for $L_b = 1$ nm, whereas for $P = 24$ kbar it is zero at $L_b = 2$ nm and $L_b = 4$ nm. Notice that for a particular electric field amplitude—in this case -10 kV/cm—, the wider the central barrier is the larger the value of the hydrostatic pressure for which $z_{11} = z_{22}$.

For high enough pressures, $P \approx 30$ kbar, the central barrier essentially disappears and the heterostructure behaves as a single quantum well (with an average width of 27 nm for the cases reported in Fig. 5). For this reason, at $P \approx 30$ kbar, the curves of $\alpha_{\max}$ converge identically and those of $\chi_{0,\max}$ have rather close values.

For $P > 10$ kbar, the growing character of $\alpha_{\max}$ is due to the augment of the effective width of the system as a function of the pressure (the central barrier height diminishes), which the consequent increase of z_{21}. Contrary to the situation of low pressures, in this case the pressure induces the growth of the value of ω_{21} which, added to the positive slope of $z_{21}(P)$, explain the growing monotonicity of $\alpha_{\max}$.

It is interesting to notice that in the dependencies of $\alpha_{\max}$ and $\chi_{0,\max}$ with the hydrostatic pressure, a zero of $\chi_{0,\max}$ does not coincide—at the same value of P—with a maximum in $\alpha_{\max}$. This is an effect that has not been previously reported in the literature. Finally, the origins of the two maxima in $\chi_{0,\max}$—for instance, when $L_b = 4$ nm—are associated to a maximum in $|\Delta z_{21}|$ and a maximum in z_{21}^2 for the left and right maximum of $\chi_{0,\max}$ respectively.

In Fig. 6 we are presenting the results of the variation of the NOA (a) and the NOR (b) resonant peaks in GaAs-$Ga_{0.7}Al_{0.3}$ As ADQW, as functions of the applied electric field, F. Notice the zero in each curve of $\chi_{0,\max}$ for negative electric fields. This zero associates with the symmetrical character of the double QW induced by the effect of the field. Under such condition we have $z_{11} = z_{22} = 0$, and therefore $|\Delta z_{21}| = 0$. At the same time, as a result of the induced symmetry in the wavefunctions, there must be a maximum of $|z_{21}|$. As it was discussed regarding Fig. 4, there appears a maximum of $\alpha_{\max}$ at precisely the same value of F for which $\chi_{0,\max}$ becomes zero.

The dominant character of z_{21}^2 tightly controls the lineshape of $\chi_{0,\max}$. Such factor reaches a well-defined maximum when the negative applied electric field induces the spatial symmetry of the states involved [compare the densities of probability in Fig. 6c, d]. This symmetry leads to a decrease of $|\Delta z_{21}| = 0$ until it becomes null. The presence of a zero in $|\Delta z_{21}| = 0$, at the very value of F that corresponds to the complete symmetry, is then responsible for the generation of the two structures that one sees in the curves of $\chi_{0,\max}$. If the applied electric fields are positive we observe a reinforcement of the asymmetry in the heterostructure. The overlap between the state wavefunctions decreases with the corresponding reduction in the term z_{21}.

As long as the central barrier width augments the value of the negative applied electric field required to induce the wavefunction symmetry is higher. This explains the shift of the zero in $\chi_{0,\max}$ towards the left hand side in Fig. 6b [compare, for example, the results for $L_b = 1$ nm and $L_b = 2$ nm]. However, an interesting and atypical case is that of $L_b = 4$ nm, which shows a displacement to the right of the zero in $\chi_{0,\max}$, with respect to the case in which the barrier width is the half of this value. This effect requires further study on the

way the electric fields can induce deformations upon the probability densities of the states involved in the transition. Work on this will be published soon.

The Fig. 7 shows the outcome of the calculation for the NOA (a) and NOR (b) resonant peak as a function of the applied magnetic field in the system under study. It is possible to see that when the pressure grows from 0 to 10 kbar, α_{max} decreases and when P goes beyond 20 kbar this peak starts being a slowly increasing function of the field. This is consistent with the results previously discussed for Fig. 5. It can also be noticed that the magnetic field turns out to be a new variable through which it is possible to induce the situation $\chi_{0,\max} = 0$ —strictly associated with the condition $z_{11} = z_{22}$. Additionally, the magnetic field at which the NOR peak is null is, at the same time, a quantity that depends on the hydrostatic pressure applied to the system.

At this point it is important to notice that when there is an augment of the coupling between the wells—due to the quenching of the central barrier height induced by the higher values of P—the strength of the magnetic field that leads to the condition $\chi_{0,\max} = 0$ must necessarily grow with pressure. Once again, we observe that $\alpha_{\max}$ presents its maximum associated with the zero of the NOR peak. Since ω_{21} is always an increasing function of the magnetic field, then the peak of the NOA and its corresponding lineshape will be strictly governed by z_{21}^2.

Initially, if $B = 0$ and the electric field is negative (applied along $+z$), the maximum of the ground state density of probability localizes within the L_{W1} well and the one corresponding to the first excited state density of probability lies mostly within the L_{W2} [see Fig. 7c]. This implies a small overlap of the wavefunctions with the consequence of a low value for z_{21}^2. By raising the magnetic field strength—given its orientation parallel to the interfaces—, the two mentioned state wavefunctions are pushed aside from each other towards opposite wells. Then, the two states show maxima of the probability density in the regions inside each QW [see Fig. 7d], which causes the increase of the wavefunctions overlap and of the value of z_{21}^2. Such an overlap grows with the augment of the magnetic field until it reaches a maximum and it reflects in a maximum of the $\alpha_{\max}$ lineshape. If the magnetic field continues its increasing we may see from Fig. 7e that the maxima of the density of probability for both states will localize within separated wells and, as it was already discussed, this has a consequence the diminishing of z_{21}^2 and $\alpha_{\max}$. This explains the fall of the latter quantity in the high magnetic fields regime.

Finally, to give an overall picture of the NOA and NOR coefficients [Eqs. (6) and (7), respectively], the Fig. 8 contains their variations as functions of the energy of the incident photon for several values of the L_{W1} QW and no external effect applied. The values of the left well width precisely coincide with those marked with white circles in Fig. 1a. It is clearly seen the influence of the geometry in the position of the resonant peaks and that there is a correlation between the heights of both peaks for a fixed geometry as it was discussed above. The redshift of the resonant peaks is strictly due to the reduction of the energy difference between the two involved states when the dimensions of the heterostructure increase. Further studies in relation with the lineshape of the NOA and NOR and the intrinsic bistability in assymetric double quantum wells under applied electric and magnetic fields and hydrostatic pressure will be published elsewhere.

Last but no least, we find appropriate to make some comments regarding one of the main approximations of our calculation model: the existence of perfectly abrupt interfaces and flat conduction bands. In fact, there will always be a band bending caused by the electrostatic interaction between electrons in the Q2D gas. The resulting form of the conduction band potential profile is obtained by self-consistently solving of the coupled Schrödinger and Poisson equations. Next we are going to discuss the main qualitative differences that would arise if the self-consistent potential would be used instead of our simpler model.

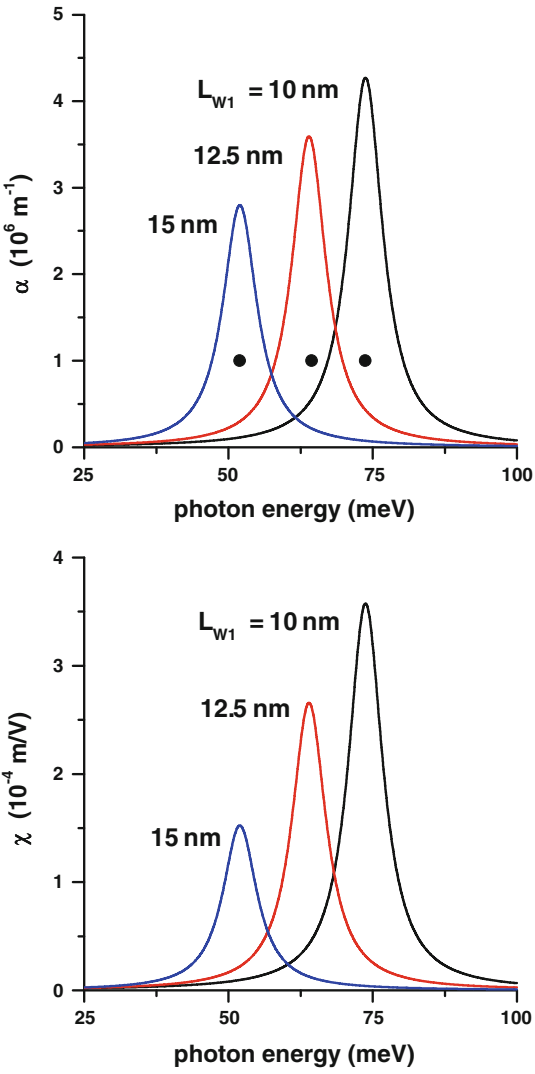

Fig. 8 Variations of the NOA (**a**) and the NOR (**b**) coefficients with the energy of the incident photon in a GaAs-$Ga_{0.7}Al_{-0.3}$ As ADQW. Calculations have been made for several values of L_{W1} with $L_{W2} = 5$ nm, $P = 0$, $F = 0$, $B = 0$, and $I/I_0 = 0.2$. The *dots* in **a** corresponds to the energy position of the resonant peaks and are exactly the same as those shown as *open dots* in Fig. 1a. (Color figure online)

First, there will be a decrease in the height of the confining potential barriers. This implies a lesser carrier confinement and, therefore, a reduction of the energy difference between the first two electron states. As a consequence, there will be a redshift for the NOR and NOA resonant peaks. This fall in the states localization allows the reinforcement of the electric field influence on them, although one always has to keep in mind that the configuration adopted includes the existence of—infinite potential—GaAs-vacuum interfaces, which at the end acts limiting the effects of F.

A significant modification would also come from the appearance of a double well configuration, generated from a single QW, due to the strong bending of the band bottom in the case of very large carrier concentrations in the gas. This would change in a rather drastic manner the energy level positions; mainly the ground state one. However, the electron densities considered in the work are small enough (10^{22} m^{-3}) as to give rise to the occupation of only

very few energy subbands. For that reason, we consider that the approximation mentioned is quite reasonable for the system under consideration. The main qualitative features can be properly described and rather small quantitative differences should really exist.

At this point, there is one issue that needs to be properly discussed here, at least qualitatively. It has to do with the limited description of the dephasing effects considered in the our calculation. The values T_1 and T_2 used for the relaxation lifetimes, related to the broadening of involved energy levels E_1 and E_2, are fixed for all possible configurations and were chosen from those reported in the literature for GaAs-based systems (Karabulut et al. 2011a; Wang and Guo 2001). The importance of dephasing in the nonlinear optical absorption has been discussed in many occasions in the literature (see, for instance, the references Ahn and Chuang 1987; Pereira et al. 1994; Pereira 2009; Schmielau and Pereira 2009). When electron densities are small enough, the phenomenon of damping in this class of materials is largely related to the scattering of charge carriers by phonons (Ahn and Chuang 1988). Such a process determines the lifetime of the electrons in the confined states. Both hydrostatic pressure and external applied fields play a significant role in the evaluation of the corresponding damping rates. These quantities induce variations in subband electron states as well as in the bulk phonon frequencies which serve as input values in the electron-phonon Hamiltonian. Furthermore, the specific interaction Hamiltonian in a low-dimensional structure is strongly dependent on the particular confining geometry of the system and the particular phonon branches involved (acoustical, optical, according to the temperature range of relevance) (Mora-Ramos 2000). A thorough evaluation of the electron-phonon-related damping rates is beyond the scope of the present work. For that reason, we have chosen to use the mentioned values of $T_{1,2}$, in order to provide a rather qualitative picture -despite the accuracy of the evaluation of single particle states in the effective mass approximation- of the nonlinear optical properties as functions of the external parameters.

Nonetheless, these limitations in our model motivate the realization of further studies on the nonlinear optical properties of asymmetrically designed semiconducting layered heterostructures, including a more accurate description of the conduction band profile via a self-consistent treatment, together with a realistic description of the dephasing effect. The relevance of these properties and systems for the development of optoelectronic devices makes them worth, and the corresponding results will be published further on.

4 Conclusions

In this work we have reported a theoretical study about the simultaneous influences of external electric and magnetic fields and hydrostatic pressure on the coefficients of nonlinear optical absorption and nonlinear optical rectification in GaAs-Al_xGa_{1-x} As asymmetric double quantum wells. The calculations use the effective mass, parabolic bands, and envelope function approximations. The main results of the work are the following: (i) in general, it is possible to obtain a maximum of the NOA coefficient for those values of the external parameters for which there is a zero in the NOR coefficient, (ii) the combination of the external electric field and the hydrostatic pressure becomes a mechanism that allows the coupling between the two QW and provides the way for controlling the position of the extremal values of the nonlinear optical properties, (iii) the lineshape of the NOR coefficient basically relates with the difference of the dipole moments of the two states involved, and it is slightly rectified by the overlap of the corresponding wavefunctions, (iv) depending on the specific regime of hydrostatic pressure, the NOA coefficient may be decreasing or increasing function of the pressure, (v) the width of the central barrier is decisive for the induction of geometry

configuration in the heterostructure with the help of the applied electric field, and (vi) the magnetic field has important effects on the overlap between the wavefunctions and consequently on the asymptotic tendencies that might be observed in the nonlinear optical rectification coefficient.

Acknowledgments CAD and MEMR thank CONACYT (Mexico) and COLCIENCIAS (Colombia) for support under the 2009–2011 Bilateral Agreement "Estudio de los efectos de la presión hidrostática y la mezcla de estados de conducción sobre la estructura electrónica y los estados excitónicos en nanoestructuras basadas en semiconductores III-V". MEMR also acknowledges support from Mexican CONACYT through grant CB-2008-101777. CAD is grateful to the Colombian Agencies CODI-Universidad de Antioquia, Facultad de Ciencias Exactas y Naturales-Universidad de Antioquia (CAD-exclusive dedication project 2011–2012), and "El Patrimonio Autónomo Fondo Nacional de Financiamiento para la Ciencia, la Tecnología y la Innovación Francisco José de Caldas" Contract RC Fb No. 275-2011. The work was developed with the help of CENAPAD-SP, Brazil.

References

Ahn, D., Chuang, S.-L.: Calculation of linear and nonlinear intersubband optical absorptions in a quantum well model with an applied electric field. IEEE J. Quantum Electron. **23**, 2196–2204 (1987)

Ahn, D., Chuang, S.-L.: Electric field dependence of the intersubband optical absorption in a semiconductor quantum well. Superlattices Microstruct. **4**, 153–157 (1988)

Baier, J., Bayanov, I.M., Plodereder, U., Seilmeier, A.: Biexponential intersubband relaxation in n-modulation-doped quantum-well structures. Superlattices Microstruct. **19**, 9–16 (1996)

Baskoutas, S., Paspalakis, E., Terzis, A.F.: Electronic structure and nonlinear optical rectification in a quantum dot: effects of impurities and external electric field. J. Phys. Condens. Matter **19**, 395024(9pp) (2007)

de Dios Leyva, M., Galindo, V.: Intraband optical absorption in superlattices in an in-plane magnetic field. Phys. Rev. B **48**, 4516–4523 (1993)

Duque, C.A., Kasapoglu, E., Şakiroglu, S., Sari, H., Sökmen, I.: Intense laser effects on nonlinear optical absorption and optical rectification in single quantum wells under applied electric and magnetic field. Appl. Surf. Sci. **257**, 2313–2319 (2011)

Duque, C.M., Mora-Ramos, M.E., Duque, C.A.: Effects of hydrostatic pressure and electric field on the nonlinear optical rectification of strongly confined electronhole pairs in GaAs quantum dots. Physica E **43**, 1002–1006 (2011)

Elabsy, A.M.: Effect of the Gamma-X crossover on the binding energies of confined donors in single $GaAs/Al_xGa_{1-x}As$ quantum-well microstructures. J. Phys. Condens. Matter **6**, 10025–10030 (1994)

Eseanu, N.: Intense laser field effect on the interband absorption in differently shaped near-surface quantum wells. Phys. Lett. A **375**, 1036–1042 (2011)

Fejer, M.M., Yoo, S.J.B., Byer, R.L., Harwit, A., Harris, J.S. Jr.: Observation of extremely large quadratic susceptibility at 9.6–10.8 μm in electric-field-biased AlGaAs quantum wells. Phys. Rev. Lett. **62**, 1041–1044 (1989)

Karabulut, I., Safak, H., Tomak, M.: Nonlinear optical rectification in asymmetrical semiparabolic quantum wells. Solid State Commun. **135**, 735–738 (2005)

Karabulut, I., Atav, U., Safak, H., Tomak, M.: Linear and nonlinear intersubband optical absorptions in an asymmetric rectangular quantum well. Eur. Phys. J. B **55**, 283–288 (2007)

Karabulut, I., Mora-Ramos, M.E., Duque, C.A.: Nonlinear optical rectification and optical absorption in $GaAsGa_{1x}Al_xAs$ asymmetric double quantum wells: Combined effects of applied electric and magnetic fields and hydrostatic pressure. J. Lumin. **131**, 1502–1509 (2011)

Karabulut, I., Duque, C.A.: Nonlinear optical rectification and optical absorption in $GaAs\text{-}Ga_{1-x}Al_xAs$ double quantum wells under applied electric and magnetic fields. Physica E **43**, 1405–1410 (2011)

Kasapoglu, E., Duque, C.A., Sari, H., Sökmen, I.: Intense laser field effects on the linear and nonlinear intersubband optical properties of a semi-parabolic quantum well. Eur. Phys. J. B **82**, 13–18 (2011)

Lien, C., Huang, Y., Wang, J.: Triply resonant enhancement of third-order nonlinear optical susceptibility in compositionally asymmetric coupled quantum wells. J. Appl. Phys. **76**, 1008(5pp) (1994)

Liu, A., Chuang, S.-L., Ning, C.Z.: Piezoelectric field-enhanced second-order nonlinear optical susceptibilities in wurtzite GaN/AlGaN quantum wells. Appl. Phys. Lett. **76**, 333(3pp) (2000)

Mora-Ramos, M.E.: A many-particle approach to the electron-phonon interaction in semiconductor nanostructures. Rev. Mex. Fis. **46**, 258–264 (2000)

Niculescu, E.C., Eseanu, N.: Interband absorption in square and semiparabolic near-surface quantum wells under intense laser field. Eur. Phys. J. B **79**, 313–320 (2011)

Pereira, M.F., Binder, R., Koch, S.W.: Theory of nonlinear optical absorption in coupled-band quantum wells with many-body effects. Appl. Phys. Lett. **64**, 279–281 (1994)

Pereira, M.F.: The influence of dephasing in the coupling of light with intersubband transitions. Microelectr. J. **40**, 841–843 (2009)

Raigoza, N., Morales, A.L., Montes, A., Porras-Montenegro, N., Duque, C.A.: Stress effects on shallow-donor impurity states in symmetrical GaAs/$Al_xGa_{1-x}As$ double quantum wells. Phys. Rev. B **69**, 045323(8pp) (2004)

Rosencher, E., Bois, P., Nagle, J., Costard, E.: Delaitre, S.: Observation of nonlinear optical rectification at 10.6 μm in compositionally asymmetrical AlGaAs multiquantum wells. Appl. Phys. Lett. **55**, 1597–1599 (1989)

Rosencher, E., Bois, Ph.: Model system for optical nonlinearities: asymmetric quantum wells. Phys. Rev. B **44**, 11315–11327 (1991)

Rosencher, E., Fiore, A., Vinter, B., Berger, V., Bois, Ph., Nagle, J.: Quantum engineering of optical nonlinearities. Science **271**, 168–173 (1996)

Sa'ar, A., Kuze, N., Feng, J., Gravé, I., Yariv, A.: Observation of third-order intersubband dc Kerr effect at the midinfrared wavelengths in GaAs quantum wells. Appl. Phys. Lett. **61**, 1263–1265 (1992)

Schmielau, T., Pereira, M.F. Jr.: Nonequilibrium many body theory for quantum transport in terahertz quantum cascade lasers. Appl. Phys. Lett. **95**, 231111(3pp) (2009)

Sirtori, C., Capasso, F., Sivco, D.L., Cho, A.Y.: Giant, triply resonant, third-order nonlinear susceptibility $X^3_{3\omega}$ in coupled quantum wells. Phys. Rev. Lett. **68**, 1010–1013 (1992)

Sirtori, C., Capasso, F., Faist, J., Pfeiffer, L.N., West, K.W.: Far-infrared generation by doubly resonant difference frequency mixing in a coupled quantum well two-dimensional electron gas system. Appl. Phys. Lett. **65**, 445–447 (1994)

Tsang, L., Chuang, S.-L., Lee, S.M.: Second-order nonlinear optical susceptibility of a quantum well with an applied electric field. Phys. Rev. B **41**, 5942–5951 (1990)

Wang, G., Guo, K.: Excitonic effects on the third-harmonic generation in parabolic quantum dots. J. Phys. Condens. Matter **13**, 8197–8206 (2001)

Wei, R., Xie, W.: Optical absorption of a hydrogenic impurity in a disc-shaped quantum dot. Curr. Appl. Phys. **10**, 757–760 (2010)

Xia, J.-B., Fan, W.-J.: Electronic structures of superlattices under in-plane magnetic field. Phys. Rev. B **40**, 8508–8515 (1989)

Xie, W.: Nonlinear optical rectification of a hydrogenic impurity in a disc-like quantum dot. Physica B **404**, 4142–4145 (2009)

Załużny, M.: Influence of the depolarization effect on the nonlinear intersubband absorption spectra of quantum wells. Phys. Rev. B **47**, 3995–3998 (1993)